Original article

Ewha Med J 2025;48(2):e30 https://doi.org/10.12771/emj.2025.00094





Development of automatic organ segmentation based on positronemission tomography analysis system using Swin UNETR in breast cancer patients: a prediction study

Dong Hyeok Choi^{1,2,3}, Joonil Hwang^{4,5}, Hai-Jeon Yoon^{6*}, So Hyun Ahn^{7,8,9*}

Purpose: The standardized uptake value (SUV) is a key quantitative index in nuclear medicine imaging; however, variations in region-of-interest (ROI) determination exist across institutions. This study aims to standardize SUV evaluation by introducing a deep learning-based quantitative analysis method that enhances diagnostic and prognostic accuracy.

Methods: We used the Swin UNETR model to automatically segment key organs (breast, liver, spleen, and bone marrow) critical for breast cancer prognosis. Tumor segmentation was performed iteratively based on predefined SUV thresholds, and prognostic information was extracted from the liver, spleen, and bone marrow (reticuloendothelial system). The artificial intelligence training process employed 3 datasets: a test dataset (40 patients), a validation dataset (10 patients), and an independent test dataset (10 patients). To validate our approach, we compared the SUV values obtained using our method with those produced by commercial software.

Results: In a dataset of 10 patients, our method achieved an auto-segmentation accuracy of 0.9311 for all target organs. Comparison of maximum SUV and mean SUV values from our automated segmentation with those from traditional single-ROI methods revealed differences of 0.19 and 0.16, respectively, demonstrating improved reliability and accuracy in whole-organ SUV analysis.

Conclusion: This study successfully standardized SUV calculation in nuclear medicine imaging through deep learning-based automated organ segmentation and SUV analysis, significantly enhancing accuracy in predicting breast cancer prognosis.

Keywords: Artificial intelligence; Breast neoplasms; Deep learning; Positron emission tomography; Prognosis; Republic of Korea

Introduction

Background

Breast cancer (BC) is the most common cancer among women and one of the leading causes of cancer-related deaths worldwide [1,2]. With recurrence rates of 20%–30%, accurate prognostic

prediction is essential for treatment planning [3]. Key prognostic factors include tumor size, nuclear grade, axillary lymph node involvement, hormone receptor status, and the Ki-67 proliferation index [4].

18F fluorodeoxyglucose positron-emission tomography/computed tomography (18F-FDG PET/CT) is widely used to evalu-

*Corresponding email: haijeon.yoon@ewha.ac.kr (Hai-Jeon Yoon) and mpsohyun@ewha.ac.kr (So Hyun Ahn)
Dong Hyeok Choi and Joonil Hwang contributed equally to this study as co-first authors.

Received: February 26, 2025 Revised: March 11, 2025 Accepted: March 26, 2025

[©] This is an open-access article distributed under the terms of the Creative Commons Attribution License (https://creativecommons.org/licenses/by nc/4.0/), which permits noncommerical use, distribution, and reproduction in any medium, provided the original work is properly cited.



e-emj.org 1 / 11

¹Department of Medicine, Yonsei University College of Medicine, Seoul, Korea

²Medical Physics and Biomedical Engineering Lab, Yonsei University College of Medicine, Seoul, Korea

³Department of Radiation Oncology, Yonsei Cancer Center, Heavy Ion Therapy Research Institute, Yonsei University College of Medicine, Seoul, Korea

⁴Department of Nuclear and Quantum Engineering, Korea Advanced Institute of Science and Technology, Daejeon, Korea

 $^{^{5}}$ Medical Image and Radiotherapy Lab, Korea Advanced Institute of Science and Technology, Daejeon, Korea

⁶Department of Nuclear Medicine, Ewha Womans University School of Medicine, Seoul, Korea

 $^{^{7}}$ Department of Biomedical Engineering, Ewha Womans University College of Medicine, Seoul, Korea

 $^{^8}$ Ewha Medical Research Institute, Ewha Womans University College of Medicine, Seoul, Korea

⁹Ewha Medical Artificial Intelligence Research Institute, Ewha Womans University College of Medicine, Seoul, Korea

 $^{\ \}odot$ 2025 Ewha Womans University College of Medicine and Ewha Medical Research Institute



ate tumor metabolism, stage cancer, and guide treatment decisions [5]. PET-derived parameters such as standardized uptake values (SUVs), metabolic tumor volume, and total lesion glycolysis (TLG) have emerged as significant prognostic indicators in BC [6,7].

Traditional segmentation methods such as region-growing, thresholding, and level-set techniques have been widely used, yet they require manual intervention and suffer from interobserver variability. The Swin UNETR model, which integrates Swin transformers with the UNETR architecture, offers improved spatial feature representation and enhanced segmentation accuracy. However, its computational cost and real-world feasibility remain areas of concern, as discussed later in this study.

Systemic inflammatory responses also influence cancer progression and prognosis [8]. Biomarkers such as the neutro-phil-to-lymphocyte ratio and platelet-to-lymphocyte ratio have been associated with outcomes in multiple cancers [9]. The reticuloendothelial system (RES), which includes the bone marrow, spleen, and liver, plays a key role in systemic inflammation. FDG PET has been used to evaluate metabolic activity in these organs, and increased RES activity has been linked to poor prognosis in BC and other cancers [10,11].

Accurate delineation of BC lesions and RES organs is essential

for quantifying PET parameters. Although manual segmentation by nuclear medicine physicians is the current gold standard, it is time-consuming and prone to interobserver variability, which can lead to potential errors [12]. Automated segmentation methods are therefore necessary to reduce variability and improve efficiency.

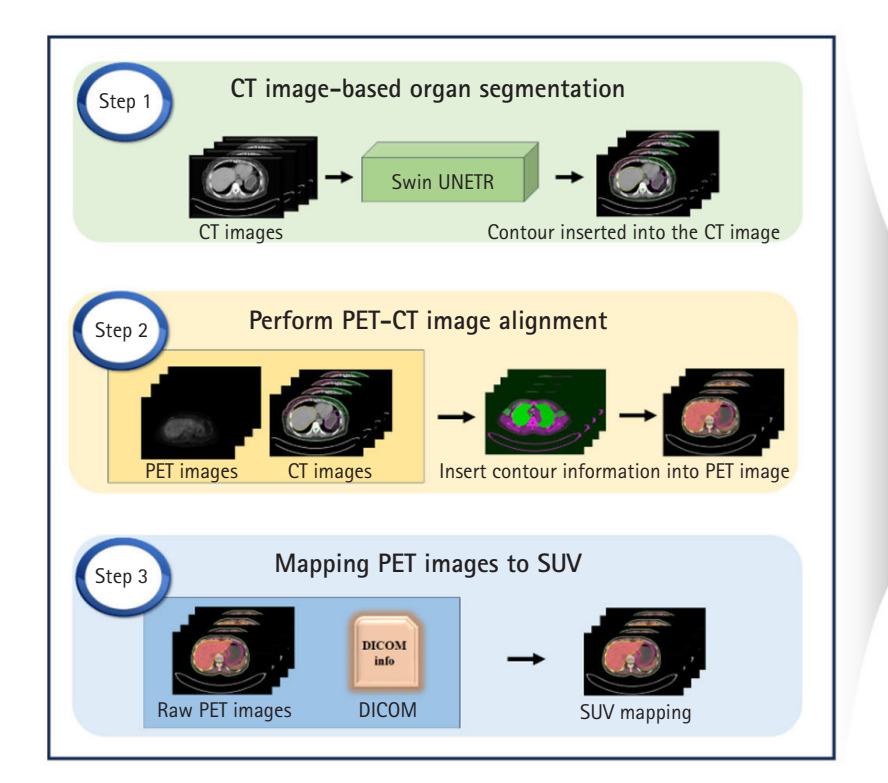
Objectives

This study employs the Swin-UNETR architecture to segment both the breast and RES organs, highlighting their prognostic significance. Our goal is to develop an advanced diagnostic and prognostic system for BC. We aimed to automate the identification of tumor location and size using SUVs derived from PET/CT scans of BC patients. In addition, we developed a computational tool to calculate SUVs in organs associated with prognosis. A schematic representation of the study flow is shown in Fig. 1.

Methods

Ethics statement

All patient data used in this research were reviewed and approved by the Institutional Review Board (IRB) of Ewha Womans University Mokdong Hospital (IRB no., 2023-07-001-002). Obtaining informed consent from individual patients was exempt be-



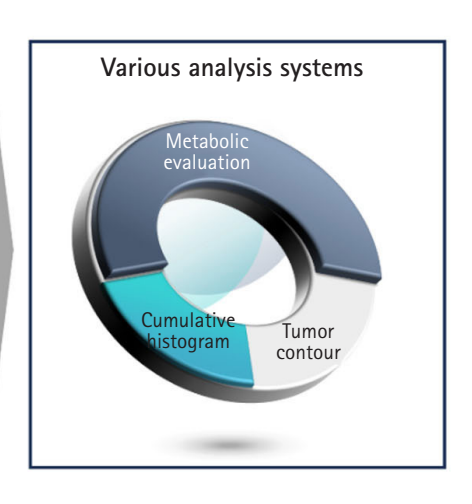


Fig. 1. Schematic representation of the study flow. The left panel summarizes the steps involved in the study, while the right panel illustrates the inherent functionalities of the research findings. CT, computed tomography; PET, positron emission tomography; SUV, standardized uptake value.

e-emj.org 2 / 11



cause of the retrospective design of this study.

Study design

This study is a retrospective, medical record-based prediction study. It is reported in accordance with the TRIPOD-artificial intelligence (AI) reporting guidelines for articles on deep learning in the medical field (development or prediction), available at https://www.tripod-statement.org/.

Setting

Data were collected between 2012 and 2014 from female patients (mean age, 54.5 ± 10.3 years; range, 33-77 years) who underwent FDG-PET/CT for initial BC staging at Ewha Womans University Mokdong Hospital in Korea.

Participants

A total of 60 patients were included in the study. All eligible patients diagnosed during the study period were included. Among them, 32 underwent mastectomy, while 28 received breast-conserving surgery.

Data source

PET/CT scans were performed using a Siemens Biograph mCT system (128-slice CT; Siemens Medical Solutions). Patients fasted for at least 6 hours before scanning, and FDG was administered when blood glucose levels were below 140 mg/dL. PET/CT images were acquired 60 minutes after an intravenous FDG injection (5.18 MBq/kg), covering the skull base to mid-thigh. First, non-contrast CT images were obtained (120 kVp, 50 mAs, 1.2 pitch), followed by 3D PET image acquisition (2 minutes per bed position, covering 5 to 7 positions). PET images were recon-

structed using a 3D-OSEM iterative algorithm (2 iterations, 21 subsets) with time-of-flight and point-spread function corrections.

Outcome variables

The outcome variables included segmentation results, PET/CT alignment, SUVs, and TLG.

Study size

No sample size estimation was performed, as all eligible subjects were included in the study.

Deep learning models

Auto segmentation

For AI model training, manual segmentation of CT scans from 60 patients was performed using MIM software (MIM Software Inc.), focusing on the breasts, liver, spleen, and bone marrow. An experienced physician performed the segmentation, which was then verified by a second experienced physician. In cases of discrepancy, the 2 physicians reached a consensus. The data were divided into a training set (40 patients), a validation set (10 patients), and an independent test set (10 patients). The Swin UN-ETR model, a deep learning architecture that integrates the Swin Transformer with convolutional neural networks, was employed for segmentation (Fig. 2).

Encoder: CT images were divided into non-overlapping $2 \times 2 \times 2$ patches, with each patch represented as a 48-dimensional feature vector. These patches were embedded into a sequence representation and tokenized at a resolution of $(H/2 \times W/2 \times D/2)$. The encoded features were processed through 2 consecutive Swin

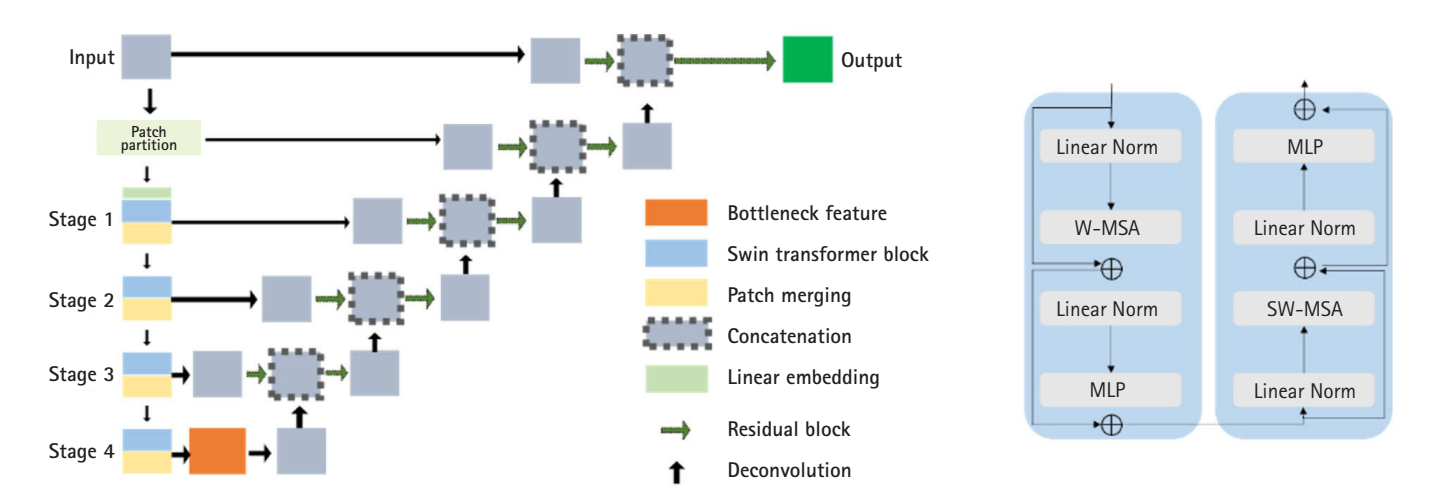


Fig. 2. The architecture (A) and transformer blocks (B) of Swin UNETR. MLP, multilayer perceptron; W-MSA, window-based multihead self-attention; SW-MSA, shifted window-based self-attention.

e-emj.org 3 / 11



Transformer blocks that utilized window-based multi-head self-attention (W-MSA) and shifted window-based self-attention (SW-MSA) (Fig. 2B). A patch-merging layer then reduced the number of tokens while doubling the feature dimensions, and this process was repeated 4 times throughout the encoding stage.

Decoder: The encoded features were reshaped to a resolution of (H/32 \times W/32 \times D/32) and processed through residual blocks comprising $3\times3\times3$ convolutional layers with instance normalization. These features were then up-sampled using deconvolutional layers and concatenated with outputs from previous stages. The final encoder output was integrated with these processed features and passed through another residual block. A final $1\times1\times1$ convolutional layer with a SoftMax activation function produced segmentation probabilities.

Model parameters: Various preprocessing techniques were employed to enhance segmentation accuracy. Pixel values were normalized between 0 and 1 by clipping those outside the range of -175 to 250. CT image resolution was standardized at $1.5 \times 1.5 \times 2.0$ mm³, and images were randomly cropped to $96 \times 96 \times 96$. Data augmentation techniques included random flipping and rotation (with a probability of 0.1) along all 3 axes, and intensity shifting (with a probability of 0.5 and an offset of 0.1). The model was trained using a combination of dice loss and cross-entropy loss, optimized with the Adam optimizer and stabilized using GradScaler (PyTorch). Training was conducted over 20,000 iterations.

SUV acquisition

PET/CT alignment: To transfer CT-based segmentation to PET images, multimodal image alignment was performed using MATLAB's alignment module. The optimizer was configured with an initial radius of 0.009, an epsilon of 1.5E-4, and a maximum of 1,000 iterations for optimal performance. Segmentation accuracy was evaluated by comparing contour coordinates from CT-based segmentation using the dice coefficient. PET contours were aligned to CT contours using MIM software, and the PET/CT alignment metric was used to assess accuracy. This analysis was conducted on 2 patients, with image details provided in Table 1.

Convert pixel values to SUVs of PET: SUVs were calculated using patient-specific parameters extracted from DICOM data

(https://www.dicomstandard.org/), including acquisition time, radiopharmaceutical start time, radionuclide half-life, total dose, rescale slope, and patient weight. These factors enabled accurate SUV quantification per voxel, facilitating metabolic activity assessment for each organ. SUVs were body weight-based and computed using the following formula:

(1)
$$\text{SUV}_{body\ weight}(\frac{kg}{cc}) = \frac{(pixel\ value\ \times Dicom\ rescale\ factor\ \times Patient\ weight)}{Total\ dose\ \times e^{(\frac{-\log(2)\times(Series\ time-Radiophamaceutical\ start\ time)}{F^{18}-F^{10}\ half\ life\ time}})$$

where pixel value represents the PET image's raw intensity, and the DICOM rescale factor normalizes the pixel arrays. "Series time" refers to the scan initiation time, while "radiopharmaceutical start time" marks the time of 18F FDG administration.

Evaluation metrics

Auto segmentation

The Swin-UNETR model was employed to segment the breasts, spleen, liver, and bone marrow. Evaluation was conducted qualitatively by comparing predicted CT images with manually labeled organ structures, and quantitatively by calculating the average dice coefficient and loss over 20,000 iterations.

Organ-level SUV evaluation

To assess the accuracy of SUV measurements, maximum SUV (SUVmax) and mean SUV (SUVmean) values were compared using different PET image analysis methods. SUVmax was extracted from each contoured organ and compared with values obtained via MIM software, ensuring that the volume of interest (VOI) excluded adjacent organs. SUVmean was evaluated using: (1) a single VOI in MIM software, (2) a single VOI in our program, and (3) A whole-organ contour in our program.

Both SUVmax and SUVmean were consistently derived across methods using a fixed 1.2 cm radius VOI centered at each organ's centroid. Statistical analysis was performed to characterize the results.

Table 1. Image size and slice thickness of the PET/CT images from 2 patients were used to verify PET/CT alignment

	Patient 1		Patient 2			
	СТ	PET	CT	PET		
Image size (pixels)	512 × 512 × 284	200 × 200 × 283	512 × 512 × 462	200 × 200 × 284		
Slice thickness (mm)	3	3	2	3		

CT, computed tomography; PET, positron emission tomography.

e-emj.org 4 / 11



Tumor contour based on SUV

Organ contour labels were aligned with PET images to localize tumors. By using registered contour labels and SUV maps, tumors were identified based on threshold values of 40% and 50% of SUV-max. This approach provided tumor coordinate information and enabled visualization of tumor size and location on CT images.

Total lesion glycolysis evaluation

TLG quantifies metabolic activity by integrating tumor size and SUV. It is calculated by multiplying each lesion's SUV by its corresponding volume and summing these values across all lesions within a given region of interest. In this study, TLG was measured using SUV thresholds of 40% and 50%.

Cumulative SUV histogram

The cumulative SUV histogram represents intertumoral heterogeneity by plotting the percentage of tumor volume that exceeds specified SUV thresholds. This method provides a concise summary of tumor metabolic characteristics. Cumulative SUV histograms were generated for all segmented organs in PET images.

Python code for this study is available at Supplement 1.

Statistical methods

Descriptive statistics were calculated.

Results

Auto segmentation

Fig. 3 presents the segmentation results for the breast, spleen,

liver, and bone marrow using the Swin-UNETR model. The left images display the organ labels, and the right images show the predicted segmentation. Fig. 4 provides quantitative results, revealing a maximum dice coefficient of 0.9311 and a minimum loss of 0.3813, which demonstrates the model's effectiveness in accurately segmenting organs with diverse shapes and sizes. These results were obtained from the validation dataset during the training process.

PET/CT alignment

A comparison of the dice scores for the CT-based contours generated by the MIM program versus our alignment program, using datasets from 2 patients, yielded dice coefficients of 0.9114 and 0.9315, respectively (Fig. 5).

SUV acquisition

SUVmax comparisons: Table 2 summarizes the SUVmax comparisons between the MIM software and our method, showing an average difference of 0.23 (range, 0.11–0.35). The liver exhibited the highest difference (0.35) due to its larger volume, whereas the spleen showed the lowest difference (0.11).

SUVmean comparisons: Table 3 presents the SUVmean comparisons. When using a single VOI, the average difference between our program and the MIM software was 0.138 (range, 0.07–0.24), with the highest variation observed in the liver (0.24) and the lowest in the right breast (0.07). When using organ contours, the difference increased to an average of 0.27 (range, 0.26–0.30), with the greatest variation in the spleen (0.30). The differences between the single VOI and organ contour methods were

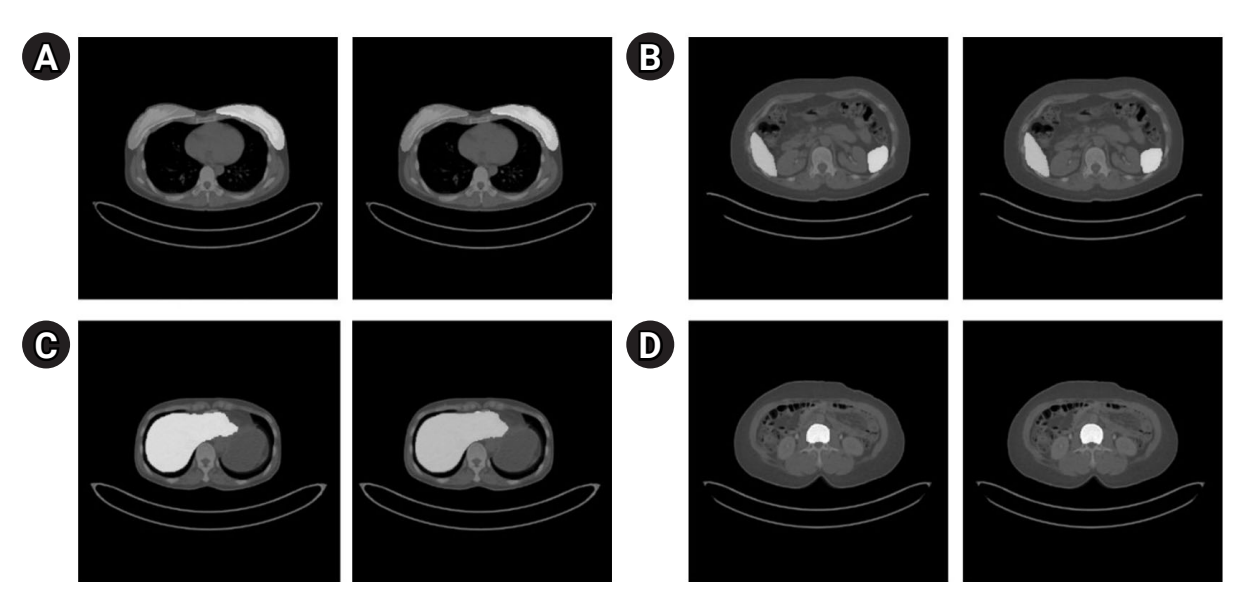


Fig. 3. Segmentation results of the Swin-UNETR model: breast (A), spleen (B), liver (C), and bone marrow (D). In each case, the left image shows the label, and the right image shows the predicted result.

e-emj.org 5 / 11



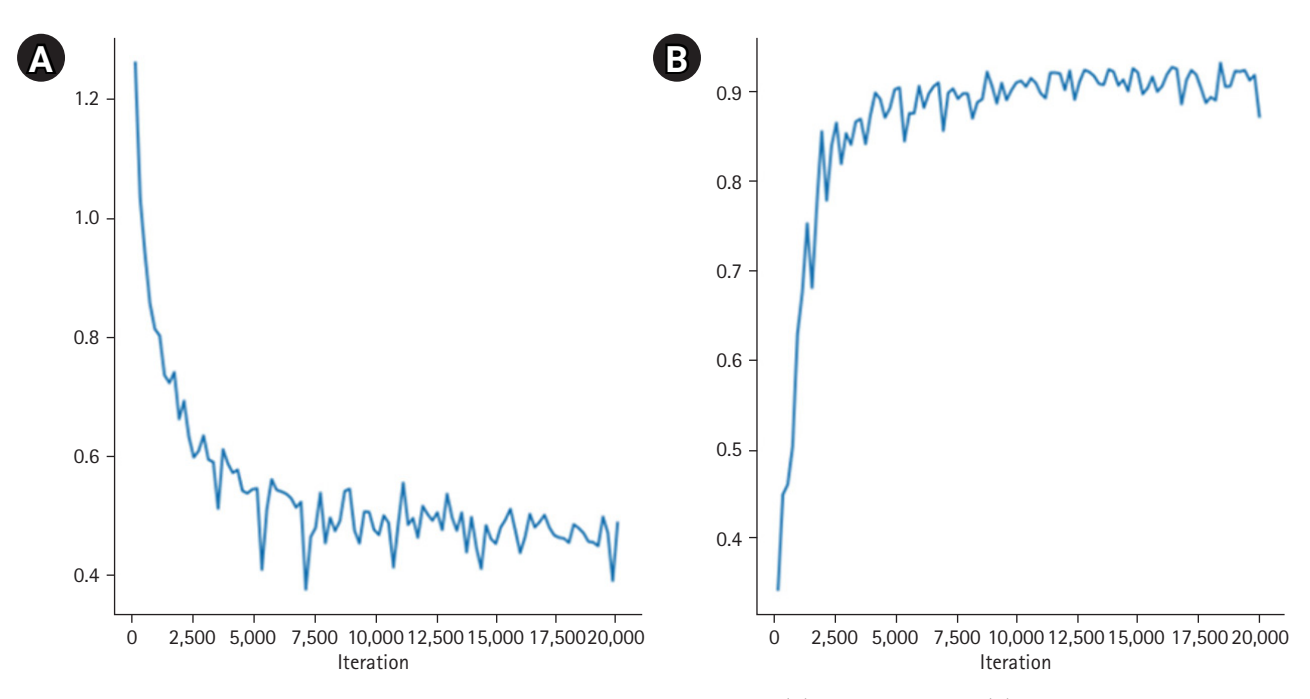


Fig. 4. Quantitative results of organ segmentation using Swin-UNETR: loss (A) and dice scores (B) during 20,000 iterations.

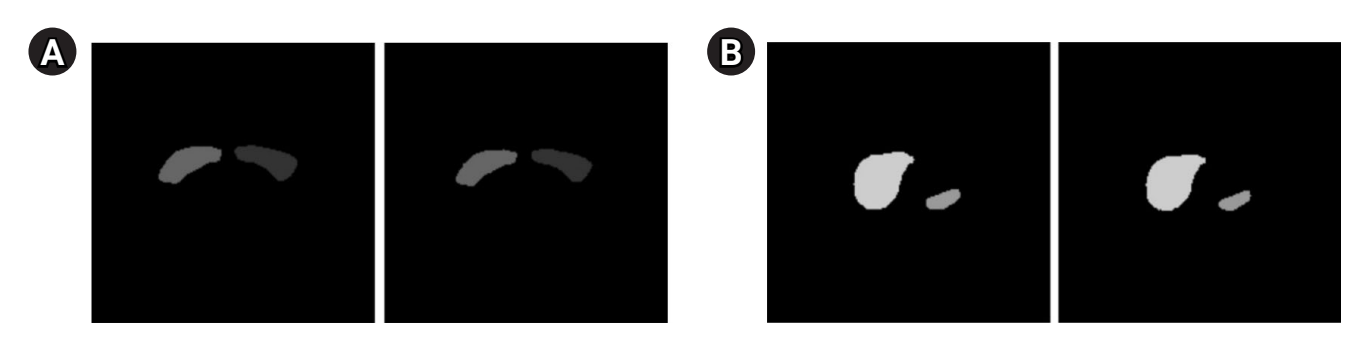


Fig. 5. Results of positron emission tomography/computed tomography alignment using the MIM program for breast (A), and liver and spleen (B). In each image, the left side displays results from the MIM program, while the right side shows results from our technique.

consistently larger than those observed between the 2 single VOI methods, highlighting the impact of VOI selection.

SUV-based tumor contour

Fig. 6 displays the results of contour-based insertion of volumetric information, specifically regions with SUVmax exceeding the 50% threshold based on BC patients' PET images. This approach enables the identification of tumor location and size on both PET and CT images.

TLG evaluation

Table 4 presents the TLG values obtained for 10 patients, focusing on the breast region where the tumors were located.

Cumulative SUV histogram

The cumulative SUV histogram was used to analyze the proportion of organ volume exceeding specific SUV thresholds. Fig. 7 shows cumulative SUV histograms for a BC patient with a right breast tumor and no lesions in the left breast. The tumor histogram exhibits a convex downward shape, indicating a higher proportion of tumor volume with SUV values above the threshold. In contrast, the healthy breast histogram shows a convex upward shape, suggesting a lower proportion of high-SUV regions.

Discussion

Key results

This study introduces a novel automated method for PET im-

e-emj.org 6 / 11



Table 2. Comparison of the SUVmax results obtained from the MIM software and our methodology

Patient index	Methods for obtaining SUVmax		Target organs				
		Breast_R	Breast_L	Liver	Spleen	Bone marrow	
1	MIM program result	12.03	1.59	2.51	1.68	1.50	
	Program results contour	11.97	1.65	2.48	1.56	1.65	
2	MIM program result	4.67	0.66	3.10	1.43	1.13	
	Program results contour	4.31	0.68	3.66	1.25	1.23	
3	MIM program result	10.96	1.96	5.43	4.47	2.60	
	Program results contour	10.79	2.18	5.98	4.71	2.74	
4	MIM program result	7.03	1.14	6.12	2.15	2.46	
	Program results contour	6.92	1.36	6.44	1.95	2.63	
5	MIM program result	1.05	7.38	2.87	2.46	2.32	
	Program results contour	0.96	7.37	3.06	2.51	2.68	
6	MIM program result	7.89	1.99	2.92	2.05	2.70	
	Program results contour	7.15	1.77	2.06	2.00	2.61	
7	MIM program result	6.91	2.54	2.38	2.14	2.29	
	Program results contour	7.55	2.77	2.18	2.10	2.18	
8	MIM program result	5.29	1.50	3.09	2.20	3.90	
	Program results contour	5.45	1.60	3.12	2.18	4.14	
9	MIM program result	4.68	2.58	6.60	3.69	3.19	
	Program results contour	5.47	2.68	6.99	3.68	3.56	
10	MIM program result	1.58	3.61	4.54	1.93	2.10	
	Program results contour	1.83	3.32	4.19	1.73	2.30	
Average difference	MIM program result-Program results contour	0.34 ± 0.27	0.15 ± 0.09	0.35 ± 0.25	0.11 ± 0.08	0.19 ± 0.10	

Values are presented as number or mean±standard deviation. Each organ was analyzed in 10 patients. SUVmax, maximum standardized uptake value.

age segmentation and quantitative evaluation based on the Swin UNETR architecture. The Swin-UNETR model achieved a dice coefficient of 0.9311 and a loss of 0.3813 for precise organ segmentation. PET/CT alignment produced dice scores of 0.9114 and 0.9315. Comparisons of SUVmax values revealed an average difference of 0.23, while SUVmean differences were 0.138 when using a single VOI and 0.27 when using organ contours. Tumor contouring successfully identified regions where SUVmax exceeded 50%. Additionally, TLG values effectively quantified tumor metabolic activity, and cumulative SUV histograms distinguished tumor tissue from healthy tissue through distinct patterns.

Interpretation/comparison with previous studies

Previous methods—including thresholding, gradient-based techniques, and region growing—suffer from limitations such as manual parameter adjustments, sensitivity to noise, and difficulty in handling complex structures [13-15]. Our approach improves segmentation accuracy by leveraging automated CT-based segmentation applied to PET images, which allows for precise organ delineation and accurate SUV extraction. By converting PET pixel values to SUVs using DICOM data, our method ensures repro-

ducibility in SUV measurements [16,17]. In contrast to conventional clinical approaches that rely on variable region-of-interest selection, our method standardizes the calculation of SUVmax and SUVmean for specific organs, thereby enhancing reliability. Moreover, analyzing SUVs from both tumor and normal tissues offers valuable predictions for postoperative outcomes, given that systemic inflammatory responses are key prognostic indicators in cancer. 18F FDG PET/CT is widely used for assessing tumor metabolism and systemic inflammation, especially in organs such as the spleen, liver, and bone marrow, which are pivotal in cancer progression.

Beyond SUV analysis, our method incorporates metabolic tumor volume and TLG, both of which are crucial for evaluating tumor burden and treatment response. By integrating SUV and tumor volume, TLG offers insights into tumor aggressiveness; if used in radiation therapy planning, this approach may lead to more effective treatment strategies.

A comparative analysis revealed differences in SUVmean values between our method and commercially available MIM software. Because MIM calculates SUVmean using a circular VOI that does not fully capture organ shape, slight variations occur. This finding

e-emj.org 7 / 11



Table 3. SUVmean results for each of the organs analyzed in 10 patients

Patient index	Methods for obtaining SUVmean	Target organs				
		Breast (right)	Breast (left)	Liver	Spleen	Bone marrow
1	MIM program result	0.76	0.74	2.18	1.30	1.23
	Program results in one VOI	0.84	0.71	1.96	1.30	1.21
	Program results contour	1.14	0.81	1.73	1.16	0.98
2	MIM program result	0.57	0.32	1.14	0.98	0.45
	Program results in one VOI	0.49	0.27	0.98	0.89	0.44
	Program results contour	0.47	0.30	1.11	0.77	0.61
3	MIM program result	1.24	1.53	1.80	2.15	1.13
	Program results in one VOI	1.28	1.40	1.85	2.02	1.17
	Program results contour	0.60	0.43	2.34	1.38	1.10
4	MIM program result	0.64	0.45	2.06	1.97	2.08
	Program results in one VOI	0.54	0.51	1.69	1.71	1.72
	Program results contour	0.59	0.45	1.67	1.48	1.37
5	MIM program result	0.55	0.45	2.19	2.12	1.32
	Program results in one VOI	0.36	0.41	1.79	1.90	1.07
	Program results contour	0.44	0.34	2.02	1.62	1.19
6	MIM program result	0.94	0.76	2.23	1.59	1.67
	Program results in one VOI	0.86	0.86	1.92	1.56	1.40
	Program results contour	0.59	0.40	1.94	1.39	1.39
7	MIM program result	1.09	0.96	1.56	1.49	0.90
	Program results in one VOI	1.13	1.58	1.80	1.66	0.80
	Program results contour	0.69	0.65	1.83	1.40	1.32
8	MIM program result	0.88	0.54	2.44	1.90	0.70
	Program results in one VOI	0.89	0.53	2.23	1.70	0.60
	Program results contour	0.50	0.38	2.13	1.45	1.34
9	MIM program result	0.32	0.41	2.42	1.90	1.77
	Program results in one VOI	0.39	0.44	2.24	2.00	1.76
	Program results contour	0.40	0.35	2.30	1.84	1.68
10	MIM program result	1.02	1.07	1.38	0.52	0.73
	Program results in one VOI	1.02	1.07	1.09	0.44	0.94
	Program results contour	0.58	0.68	1.32	0.58	0.75
Average difference	MIM program result; program results in one VOI	0.07 ± 0.05	0.11 ± 0.18	0.24 ± 0.10	0.13 ± 0.08	0.14 ± 0.12
	MIM program result; program results contour	0.29 ± 0.19	0.26 ± 0.31	0.26 ± 0.16	0.30 ± 0.23	0.27 ± 0.23

Values are presented as number or mean±standard deviation. A comparison of the SUVmean results obtained using the MIM program and our methodology using a single VOI, with the SUVmean obtained from the contoured organs shown. SUVmean, mean standardized uptake value; VOI, volume of interest.

emphasizes the importance of precise VOI selection and contouring techniques when evaluating SUVs, especially for SUVmean calculations.

Higher TLG values indicate increased glycolytic activity, suggesting greater tumor aggressiveness, and underscore TLG's value as a biomarker for BC tumor burden and metabolic characteristics. By quantifying metabolic activity, TLG provides valuable information for treatment planning and monitoring.

Although TLG findings are clinically significant, our current study does not include follow-up data on tumor recurrence or patient mortality. Future research will evaluate the correlation between TLG and clinical outcomes by incorporating both short-term data for recurrence assessment and long-term data for survival analysis, thereby providing deeper insights into the prognostic value of TLG in BC management.

Limitations

Inter-observer agreement could not be assessed because segmentation was performed by a single physician and subsequently verified by another, rather than being conducted independently by multiple annotators. This approach may introduce potential bias in the segmentation process. Future studies that include mul-

e-emj.org 8 / 11



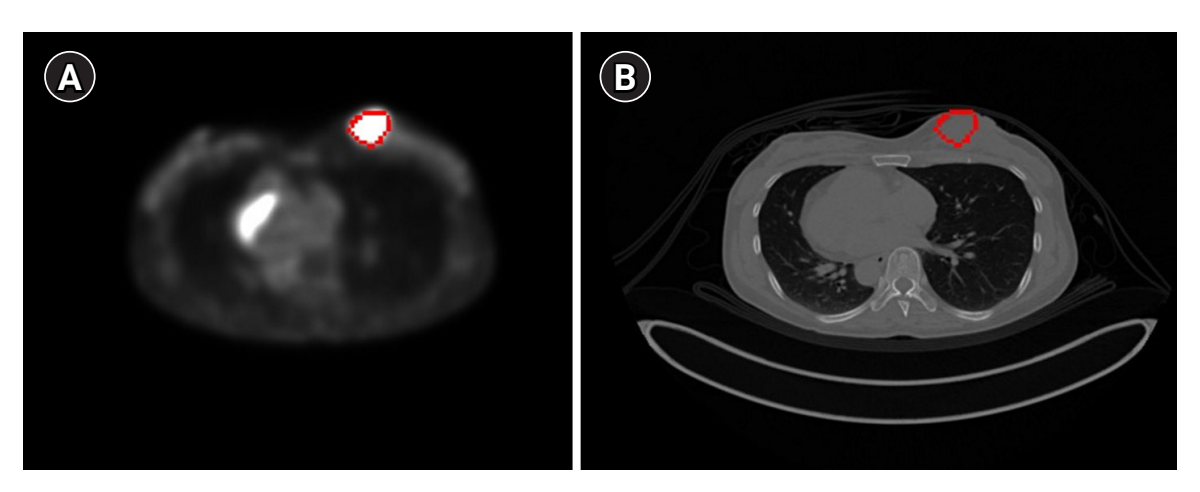


Fig. 6. The tumor with a maximum standardized uptake value greater than the 50% threshold displayed on a breast cancer (BC) positron emission tomography image (A) and a BC computed tomography image (B) using the contour method.

Table 4. Tumor locations and their TLG values in the 10 patients

Patient index	Donat annual anti-	TLG			
	Breast cancer location	Threshold (40%)	Threshold (50%)		
1	Right breast cancer in the inner pericentral area	5,794	4,551		
2	Right breast cancer in the upper pericentral area	1,714	1,382		
3	Right breast cancer in the upper outer area	1,185	889		
4	Right breast cancer in the lower center area	1,898	1,296		
5	Left breast cancer in the upper outer area	2,052	1,004		
6	Right breast cancer in the lower pericentral area	3,098	1,893		
7	Right breast cancer in the lower pericentral area	3,513	2,586		
8	Right breast cancer in the upper outer area	1,358	733		
9	Metastatic lymph node in the right axilla	383	275		
10	Left breast cancer in the upper outer area	2,909	2,216		

TLG was calculated by setting the maximum SUV threshold at 40% and 50% and calculating the mean SUV.

TLG, total lesion glycolysis; SUV, standardized uptake value.

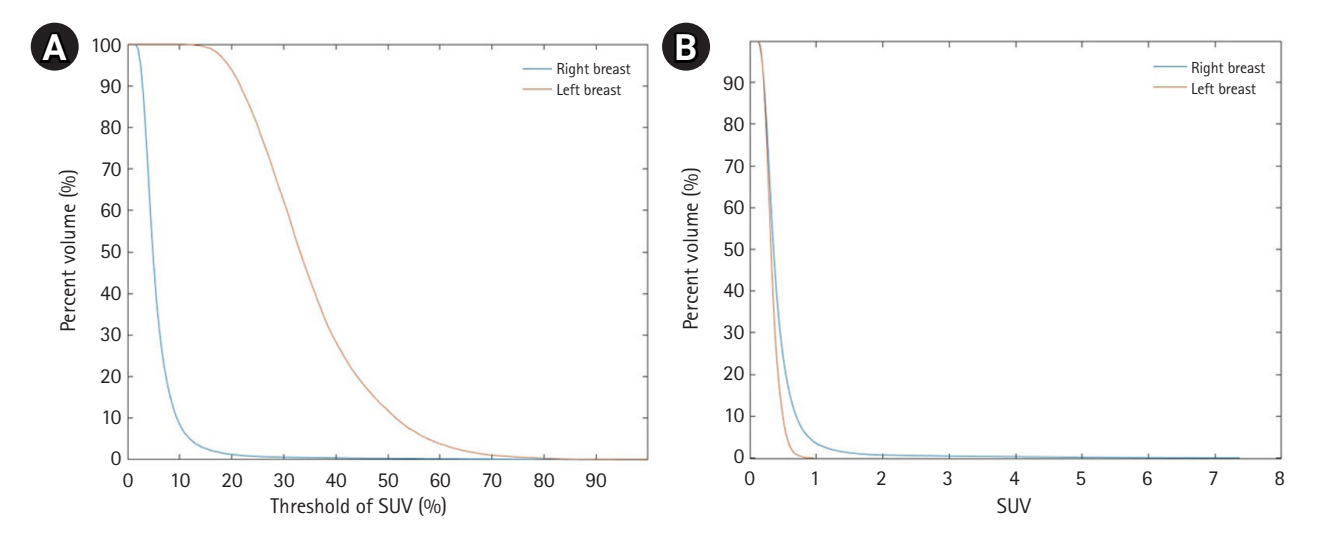


Fig. 7. Cumulative standardized uptake value (SUV) histogram results for a breast cancer patient with a tumor in the right breast. (A) The x-axis represents the SUV threshold (%) and (B) the x-axis represents absolute SUV values.

e-emj.org 9 / 11



tiple independent annotations and calculate agreement metrics could further validate the robustness of this segmentation methodology.

Clinical implications

Our method offers several clinical advantages. Automated PET segmentation facilitates early cancer detection and diagnosis while improving treatment planning. Quantitative metabolic lesion evaluation using SUVs and TLG functions as an independent prognostic factor that improves patient stratification and monitoring. Additionally, our approach reduces inter-observer variability, streamlines workflow, and enhances the efficiency of image interpretation, ultimately leading to better patient management.

Although the training phase of the Swin UNETR model requires substantial computational resources, the inference process—where the trained model segments new scans—is highly efficient and can be completed within seconds per scan. If further validated, this approach could be integrated into clinical programs to support automated segmentation. Moreover, applying optimization techniques such as model pruning and mixed-precision inference could further enhance its real-time applicability in clinical workflows. While this study focuses on the feasibility of using Swin UNETR for segmentation and SUV quantification, the impact of variations in SUV calculation methods on clinical decision-making remains to be fully understood. Future research should investigate how these variations influence prognosis prediction and treatment response assessment, thereby confirming its practical utility in clinical workflows.

Suggestion for further studies

Despite the demonstrated benefits, challenges persist in cases with a low signal-to-noise ratio or atypical PET images. Further optimization is required to minimize errors during the transfer of CT-based contours to PET images. Additionally, we plan to extend the segmentation to include the lungs and lymph nodes—common metastatic sites in BC—to improve metastasis detection and prognosis prediction. Future research will concentrate on refining the algorithm's performance and expanding its capabilities to manage more complex cases.

Conclusion

This study introduces an automated PET segmentation and evaluation method that enhances diagnostic accuracy and supports treatment planning in BC patients. Further optimization is needed to address remaining segmentation challenges and to broaden its clinical applications.

ORCID

Dong Hyeok Choi: https://orcid.org/0000-0002-5520-732X Joonil Hwang: https://orcid.org/0009-0002-7746-2433 Hai-Jeon Yoon: https://orcid.org/0000-0001-8752-6280 So Hyun Ahn: https://orcid.org/0000-0002-0116-3325

Authors' contributions

Conceptualization: HJY, SHA. Data curation: DHC, JH, HJY. Methodology, Formal analysis, validation: JH, HJY. Project administration: HJY. Funding acquisition: SHA. Writing–original draft: DHC, JH. Writing–review & editing: DHC, HJY, SHA.

Conflict of interest

So Hyun Ahn has been an assistant editor since August 2023; however, she was not involved in the peer review process. No other potential conflict of interest relevant to this article was reported.

Funding

This work was supported by the National Research Foundation (NRF), funded by the Korea government(MSIT) (RS-2024–00453521 and NRF-2020R1A5A2019210).

Data availability

The datasets generated during and/or analyzed during the current study are available from the corresponding author on reasonable request.

Acknowledgments

None.

Supplementary materials

Supplement 1. Python code used in this study is available at https://github.com/DonghyeokChoi/breast_pet.git

References

- Sung H, Ferlay J, Siegel RL, Laversanne M, Soerjomataram I, Jemal A, Bray F. Global cancer statistics 2020: GLOBOCAN estimates of incidence and mortality worldwide for 36 cancers in 185 countries. CA Cancer J Clin 2021;71:209-249. https://doi.org/10.3322/caac.21660
- Na KY, Kim KS, Lee JE, Kim HJ, Yang JH, Ahn SH, Moon BI, Kim RM, Ko SM, Jung YS. The 70-gene prognostic signature for Korean breast cancer patients. J Breast Cancer 2011;14:33-38. https://doi.org/10.4048/jbc.2011.14.1.33
- 3. Jung NY, Kim SH, Choi BB, Kim SH, Sung MS. Associations between the standardized uptake value of (18)F-FDG PET/

e-emj.org 10 / 11



- CT and the prognostic factors of invasive lobular carcinoma: in comparison with invasive ductal carcinoma. World J Surg Oncol 2015;13:113. https://doi.org/10.1186/s12957-015-0522-9
- **4.** Geus-Oei LF, Oyen WJ. Predictive and prognostic value of FDG-PET. Cancer Imaging 2008;8:70-80. https://doi.org/10.1102/1470-7330.2008.0010
- 5. Wen W, Xuan D, Hu Y, Li X, Liu L, Xu D. Prognostic value of maximum standard uptake value, metabolic tumor volume, and total lesion glycolysis of positron emission tomography/computed tomography in patients with breast cancer: a systematic review and meta-analysis. PLoS One 2019;14:e0225959. https://doi.org/10.1371/journal.pone.0225959
- 6. Pak K, Seok JW, Kim HY, Nguyen TL, Kim K, Kim SJ, Kim IJ, Hopper J. Prognostic value of metabolic tumor volume and total lesion glycolysis in breast cancer: a meta-analysis. Nucl Med Commun 2020;41:824-829. https://doi.org/10.1097/MNM. 0000000000001227
- 7. Hanahan D, Weinberg RA. Hallmarks of cancer: the next generation. Cell 2011;144:646-674. https://doi.org/10.1016/j.cell. 2011.02.013
- 8. Kim YI, Kim YJ, Paeng JC, Cheon GJ, Lee DS, Chung JK, Kang KW. Prediction of breast cancer recurrence using lymph node metabolic and volumetric parameters from 18F-FDG PET/CT in operable triple-negative breast cancer. Eur J Nucl Med Mol Imaging 2017;44:1787-1795. https://doi.org/10.1007/s00259-017-3748-7
- Proctor MJ, Talwar D, Balmar SM, O'Reilly DS, Foulis AK, Horgan PG, Morrison DS, McMillan DC. The relationship between the presence and site of cancer, an inflammation-based prognostic score and biochemical parameters: initial results of the Glasgow Inflammation Outcome Study. Br J Cancer 2010; 103:870-876. https://doi.org/10.1038/sj.bjc.6605855

- Roxburgh CS, McMillan DC. Role of systemic inflammatory response in predicting survival in patients with primary operable cancer. Future Oncol 2010;6:149-163. https://doi.org/ 10.2217/fon.09.136
- Guthrie GJ, Charles KA, Roxburgh CS, Horgan PG, McMillan DC, Clarke SJ. The systemic inflammation-based neutrophil-lymphocyte ratio: experience in patients with cancer. Crit Rev Oncol Hematol 2013;88:218-230. https://doi.org/10.1016/j.critrevonc.2013.03.010
- 12. McMillan DC. The systemic inflammation-based Glasgow Prognostic Score: a decade of experience in patients with cancer. Cancer Treat Rev 2013;39:534-540. https://doi.org/10.1016/j.ctrv.2012.08.003
- 13. Geets X, Lee JA, Bol A, Lonneux M, Gregoire V. A gradient-based method for segmenting FDG-PET images: methodology and validation. Eur J Nucl Med Mol Imaging 2007;34: 1427-1438. https://doi.org/10.1007/s00259-006-0363-4
- 14. Paulino AC, Johnstone PA. FDG-PET in radiotherapy treatment planning: pandora's box? Int J Radiat Oncol Biol Phys 2004;59:4-5. https://doi.org/10.1016/j.ijrobp.2003.10.045
- 15. Pieczynski W. Markov models in image processing. Trait Signal 2003;20:255-278.
- 16. Matheoud R, Ferrando O, Valzano S, Lizio D, Sacchetti G, Ciarmiello A, Foppiano F, Brambilla M. Performance comparison of two resolution modeling PET reconstruction algorithms in terms of physical figures of merit used in quantitative imaging. Phys Med 2015;31:468-475. https://doi.org/10.1016/j.ejmp. 2015.04.011
- 17. Pierce LA 2nd, Elston BF, Clunie DA, Nelson D, Kinahan PE. A digital reference object to analyze calculation accuracy of PET standardized uptake value. Radiology 2015;277:538-545. https://doi.org/10.1148/radiol.2015141262

e-emj.org 11 / 11